ACS APPLIED MATERIALS & INTERFACES

Research Article

www.acsami.org

Colloidally Stable and Surfactant-Free Protein-Coated Gold Nanorods in Biological Media

Moritz Tebbe,[†,§] Christian Kuttner,[†,§] Max Männel,[†] Andreas Fery,[†] and Munish Chanana*[,†,‡]

[†]Physical Chemistry II, University of Bayreuth, 95447 Bayreuth, Germany

[‡]Institute of Building Materials, ETH Zurich, 8093 Zurich, Switzerland

Supporting Information

ABSTRACT: In this work, we investigate the ligand exchange of cetyltrimethylammonium bromide (CTAB) with bovine serum albumin for gold nanorods. We demonstrate by surface-enhanced Raman scattering measurements that CTAB, which is used as a shape-directing agent in the particle synthesis, is completely removed from solution and particle surface. Thus, the protein-coated nanorods are suitable for bioapplications, where cationic surfactants must be avoided. At the same time, the colloidal stability of the system is significantly increased, as evidenced by spectroscopic investigation of the particle longitudinal surface plasmon resonance, which is sensitive to aggregation. Particles are stable at very high concentrations (c_{Au} 20 mg/mL) in biological media such as phosphate buffer saline or Dulbecco's Modified Eagle's Medium and over a large pH range (2−12). Particles can even be freeze-dried (lyophilized) and redispersed. The protocol was applied to gold nanoparticles with a large range of aspect ratios and sizes with main absorption frequencies covering the visible and the near-IR spectral range from 600 to 1100 nm. Thus, these colloidally stable and surfactant-free protein-coated nanoparticles are of great interest for various plasmonic and biomedical applications.

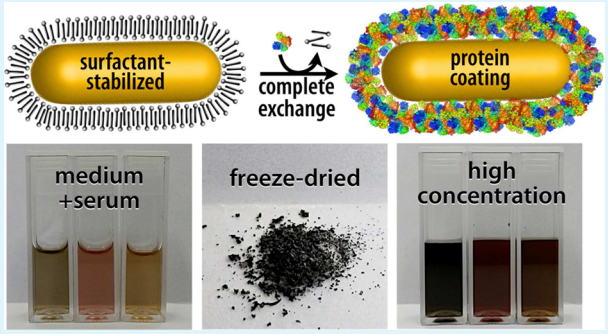

KEYWORDS: *ligand exchange, protein coating, colloidal stability, CTAB replacement, biocompatible, lyophilized*

INTRODUCTION

Gold nanorods (AuNRs) belong to a highly interesting class of nanosized objects used for a plethora of biomedical and biotechnological applications such as sensing,[1] imaging,[2−4] and others.[5] Their local surface plasmon resonances (LSPRs) strongly depend on their shape and dimensions (size, aspect ratio). Especially in the case of AuNRs with higher aspect ratios (AR > 4), the longitudinal LSPR is located in the so-called "water transparency window" in the near-IR (NIR, 800−1300 nm), where absorption of biomatter is low, thus showing potential in a wide variety of biological applications (e.g., biolabeling or hyperthermia). Along with some other additives, cetyltrimethylammonium bromide (CTAB) is the most widely used compound for the precise synthesis of AuNRs with different lengths and aspect ratios. Even though such gold nanoparticles (AuNPs) exhibit optimal optical properties for biomedical applications, their application in biomedicine is restricted due to the presence of CTAB, which is cytotoxic above a concentration of 1−10 μM.[6] In addition to this problem, CTAB-stabilized particles suffer from low colloidal stability in aqueous salt solutions, incompatibility with other solvents, and instability in long-term storage (which result in crystallization of CTAB and morphology loss upon reshaping).[7]

Many efforts have thus been made to replace CTAB in synthesis or to functionalize CTAB-coated AuNRs.[8−14] Various strategies have been developed to improve the stability and biocompatibility of AuNRs by using polymers,[15−17] peptides,[18] surfactants,[19] and lipids[13,20,21] to modify the NP surface. Most of these strategies use thiolated molecules or electrostatic interaction forces to bind to the gold surface. However, the majority of the applied coating materials are based on either simple surfactants, such as oleic acid or end-thiolated CTAB,[14] or on polymers, such as different polyelectrolytes,[9] PEG,[22−25] or polystyrene.[26] Also inorganic coatings such as silica shells have been used.[22,27] Current applications demand a combination of colloidal stability, biocompatibility, and access to further functionalization, and stimulus responsiveness. Even though many of the above-mentioned systems suffice some of these requirements, there is still a need for such multifunctional coatings.

In this context, proteins represent a promising class of multifunctional coating material.[28−31] Proteins offer a chemically well-defined structure with various chemical functionalities such as thiols, amines, and carboxylates that have high binding affinity toward metal surfaces.[28,32] Furthermore, they are high-molecular-weight charged polymers, which provide electrosteric stabilization and pH-responsiveness to the particles.[28−31]

Received: January 13, 2015
Accepted: February 23, 2015
Published: February 23, 2015

DOI: 10.1021/acsami.5b00335
ACS Appl. Mater. Interfaces 2015, 7, 5984−5991

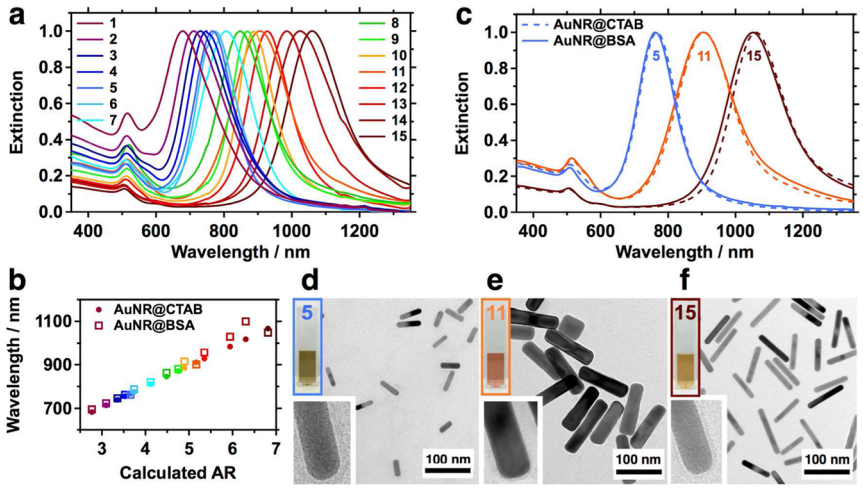

Figure 1. (a) UV−vis−NIR spectra of all AuNR@CTAB. (b) L-LSPRs of AuNR before and after BSA coating. (c) UV−vis−NIR spectra of three selected AuNR samples (Nos. 5, 11, and 15) before and after BSA coating. (d−f) TEM images of the AuNR@BSA from (c).

We recently reported on the protein coating of different spherical AuNPs with citrate and CTAB as stabilizing agents for their use as dual-responsive NPs. However, functionalization of nanorods with proteins is not straightforward, owing to destabilization and consequently strong irreversible aggregation of AuNRs during the functionalization process. In general, the functionalization of high aspect ratio NPs with polymers stays a challenge.[1,33−35] Because of the large side-to-tip area ratio and the large surface-to-volume ratio compared to spherical systems, functionalization of CTAB-stabilized AuNRs is more demanding.[14] CTAB binds relatively weakly on the tips of an AuNR and much stronger on the sides of the AuNR, since those expose different crystallographic planes.[36−38] This fact, which is exploited in the synthesis for shape directing, is problematic within the exchange. The CTAB molecules on the tips are exchanged first, causing imbalance in the CTAB bilayer structure on the rod surface. Because of this two-step exchange process, bilayer structure breaks down and results in fast AuNR aggregation. Hence, it is important to exchange the whole CTAB bilayer at once, rather than in two steps, to overcome or avoid the aggregation process.[1]

Furthermore, considering the relevant bioapplications, CTAB must be removed completely both from the solution and particle surface. In our previous report, the question whether the negatively charged protein coating adsorbs on top of the positively charged CTAB bilayer via electrostatic interactions or replaces the CTAB molecules partially or completely remains unanswered.

Hence, in this work, we report on replacing CTAB completely from AuNRs of variable aspect ratios with bovine serum albumin (BSA) without affecting the colloidal stability of the AuNRs but rather enhancing it significantly. We show the complete removal of CTAB from the particle surface employing surface-enhanced Raman scattering (SERS) measurements. We analyze the impact of protein coating on colloidal stability using the characteristic spectroscopic features of the longitudinal localized surface plasmon resonance (L-LSPR), which is highly sensitive toward aggregation. Finally we investigate freeze-drying and redispersion properties of the BSA-coated AuNRs.

RESULTS AND DISCUSSION

Figure 1 presents an overview of the spectroscopic properties and morphology of the nanorods synthesized in this study. The AuNRs were prepared following two synthetic approaches reported elsewhere.[39−41] Combining both synthesis methods allows for covering the visible and the NIR spectral range from 600 to 1100 nm with L-LSPR of the NRs (see Figure 1a).

For the coating of CTAB-stabilized AuNRs with BSA, we modified substantially our previously reported protein coating procedure for CTAB-stabilized gold nanospheres (AuNS).[29] Prior to the ligand exchange of AuNRs, the CTAB concentration of the dispersions was adjusted to 0.1 mM right before functionalization, which is by a factor of ten below the CMC of CTAB (1 mM). Please note, NP concentrations are kept the same as in the original synthesis. The AuNRs are stable for short time at this CTAB concentration; therefore, it is crucial to adjust the CTAB concentration directly prior to exchange. The AuNR dispersions are added to a relatively highly concentrated protein solution (10 mg/mL) at pH 7 under vigorous stirring and sonication (BSA solution/NP dispersions, 3:1 v/v). The mixture was sonicated for another 30 min and then centrifuged. The supernatant was replaced by the same amount of a basic and less-concentrated protein solution (1 mg/mL, pH 12) and incubated for at least 24 h. Subsequently, the AuNR dispersions were washed with basic water (pH 11−12, at least three times) via centrifugation and concentrated to desired values.

For a successful and aggregation-free BSA coating of AuNRs, CTAB must be replaced fast and completely from the surface. Hence, the ligand-exchange process on the surface must be fast and efficient. In the procedure presented here, this is presumably achieved by the interplay of intrinsic properties of the protein and the chosen experimental parameters. Hereby, three main aspects play an important role: First, the high BSA-to-CTAB ratio throughout the process results in a strong shift of equilibrium toward BSA-coated particles, which is in agreement with theory.[42] Second, BSA exhibits a higher binding affinity toward metal surfaces because BSA, as a protein, is a multivalent ligand compared to CTAB, which is a monovalent ligand. Third, the released CTAB (positively charged, hydrophobic tail) builds a complex with the excess BSA (negatively charged, hydrophobic core) in the solution and is removed efficiently from the solution in the first centrifugation steps. Hence, by adjusting the CTAB concentration far below the CMC, using high BSA concentrations (10 mg/mL) and fast destabilization of CTAB bilayer by ultra-

DOI: 10.1021/acsami.5b00335
ACS Appl. Mater. Interfaces 2015, 7, 5984−5991

sonciation in the presence of unbound BSA, a complete and aggregation-free BSA coating of AuNRs can be ensured.

The colloidal stability after the different coating procedure steps was monitored via UV−vis−NIR spectroscopy. The functionalized nanorods were also characterized by transmission electron microscopy (TEM). Figure 1b shows the results for BSA-coating of all the different AuNR samples. For clarity, the extinction spectra (Figure 1c) and TEM images (Figure 1d−f) of three representative AuNR dispersions (Figure 1d−f insets) with increasing aspect ratios (ARs) are shown. By comparing the position of the L-LSPR (Figure 1b), the shape of the extinction spectra (Figure 1c), and the color of the dispersions (Figure 1d−f insets), the aggregation-free coating of the AuNRs with BSA can be confirmed. In the case of any aggregation, the LSPR peak of the plasmonic NPs would shift drastically toward higher wavelengths, and the whole LSPR band would broaden significantly along with a decrease in overall intensity.[43] The L-LSPR of the low AR AuNRs (Figure 1b, Nos. 1−7) exhibit a spectral shift of only few nanometers, attributed to the local refractive index changes in the vicinity of the gold surface. The LSPR band also does not change in shape, revealing no aggregation during the coating process. Thus, successful ligand exchange (coating) without aggregation of the AuNRs is demonstrated. In the case of the high AR AuNRs (Figure 1b, Nos. 8−15), the L-LSPR lies in the NIR range and is therefore more sensitive toward changes in refractive index.[44−46] Sample Nos. 12−14 exhibit a more pronounced red-shifted L-LSPR after BSA coating and purification, while sample Nos. 11 and 15 are slightly blue-shifted. Changes in LSPR reflect changes in composition of AuNR ensembles. Consequently the purification of the AuNRs via centrifugation can have a huge impact on the final quality and therefore on the LSPR band of AuNRs ensembles. Harsh centrifugation can cause nanoparticle aggregation, which leads to a broadening and a red shift of the LSPR. At the same time gentle centrifugation can cause a narrowing of the dispersity and L-LSPR, owing to the size- and shape-dependent sedimentation coefficients of anisotropic NPs (centrifugation speeds can be found in Experimental Section). In our case aggregation of AuNRs can be excluded, since the shape and the overall peak width of the LSPR band is not changing significantly as it can be seen from Figure 1c and the full-width half-maximum (FWHM) values before and after functionalization (Figure S1 in the Supporting Information). The AuNR@BSA samples are remarkabely stable over time (months), without any sign of aggregation (Supporting Information, Figure S3).

As mentioned in the Introduction, the prerequisite for any biomedical application of colloidal particles is their colloidal stability under physiological salt concentrations (equivalent to 150 mM NaCl) and in complex biofluids, which contain sugars and proteins. Hence, the colloidal stability of three selected AuNR samples (Nos. 5, 11, and 15) coated with BSA (Figure 2a) was investigated in aqueous solutions at different conditions, including phosphate-buffered saline (PBS) solutions and Dulbecco's Modified Eagle's Medium (DMEM) cell culture media with 10% newborn bovine calf serum (NCS). The colloidal stability of the AuNRs in medium was again monitored by UV−vis−NIR spectroscopy (Figure 2). Remarkably, the AuNR@BSA samples were highly stable in these media over time (Supporting Information, Figure S4). Please note that such protein-coated NPs are even more stable in the presence of free protein in the solution.[30] The AuNR@BSA

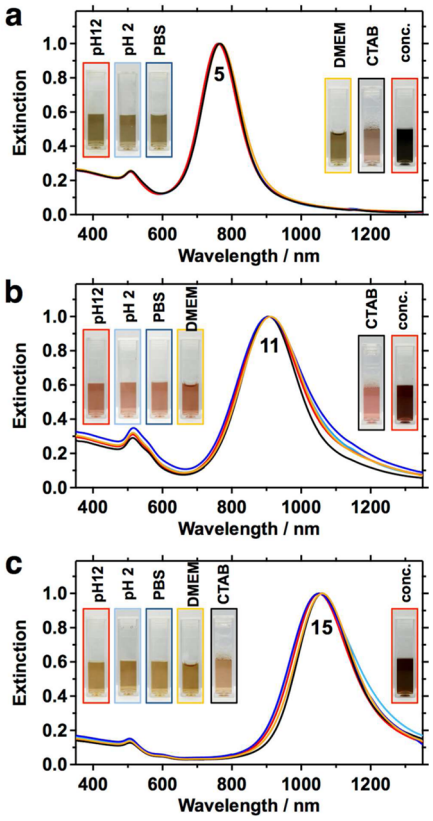

Figure 2. UV−vis−NIR spectra and photographs of three selected AuNRs, namely, (a) No. 5 at 760 nm, (b) No. 11 at 900 nm, and (c) No. 15 at 1050 nm dispersed in different media: AuNR@BSA samples (c_{Au} = 0.2 mM) were dissolved at different pH (12 and 2), in PBS buffer (150 mM, pH 7.5), in DMEM+10% NCS (pH 7.5), and highly concentrated (1 mM). AuNR@CTAB samples are included for comparison.

were also highly stable at pH values above, as well as below, the isoelectric point of BSA (pI_{BSA} = 4.8).[29] They exhibited a negative surface charge ($\zeta < -35$ mV) at pH 12 and a positive surface charge ($\zeta > +20$ mV) at pH 1, consistent with the values reported for BSA-coated NPs previously.[29]

For dosage, storage, transportation, and material handling, a dry powder form is advantageous as compared to a solution. Particularly in biomedical applications, the dose of such nanoparticles must be precisely adjusted, which can be easily done by weighing the dry sample. Drying a nanomaterial to powder and redispersing it in desired media at desired concentrations, without inducing irreversible particle aggregation during the drying or redispersion process, is highly challenging. In our case, lyophilized powders of purified dispersions (free of unbound protein and other solutes) exhibited hydrophobic properties and did not redisperse in aqueous media (see Supporting Information, Figure S2). The reason for this is that proteins pose intrinsically a demanding challenge to achieve successful lyophilization due to their denaturation during freeze-drying.[47] To avoid irreversible denaturation of proteins, hydrogen bond-forming stabilizers (lyoprotectors) such as sugars (sucrose, trehalose) or proteins such as albumins are employed. This also applies to the protein-coated nanoparticle systems. Thus, we freeze-dried our dispersions using different formulations and obtained dark brown lyophilized powders. In particular, we lyophilized purified NPs (washed 5×, pH 12), with and without

DOI: 10.1021/acsami.5b00335
ACS Appl. Mater. Interfaces 2015, 7, 5984−5991

lyoprotecting additives. We employed sucrose as a low-molecular-weight sugar-based additive and BSA itself as a high-molecular-weight protein-based additive. Furthermore, we also employed DMEM and DMEM containing 10% NCS as formulation media for the lyophilization. Depending on the formulation the AuNR@protein powders exhibited different solubility behavior upon redispersion in water, buffers, and medium.

Whereas the powders from the formulations that contained lyoprotectors redispersed readily in water (pH > 7) and buffers as well as cell culture media, the powders from the water formulation (pH 12), which contained no stabilizing additives, were not redispersible (see Supporting Information, Figure S2). The powder from the water formulation remained as a clump at the air−water interface or rather stuck to the walls of the vial showing a hydrophobic character of the lyophilized protein coating. The powders containing lyoprotecting agents, on the other hand, exhibited remarkable redispersion behavior. Powders from the formulations containing sucrose (1 mg/mL) or BSA (1 mg/mL) both redispersed spontaneously in aqueous media. The redispersion behavior upon addition of Milli-Q water at pH 12 was documented in Videos V1 and V2, provided in the Supporting Information. These dispersions of the freeze-dried AuNR@BSA were also highly stable over time periods of weeks and months (Supporting Information, Figure S5). Here, the dispersions were identical to the original AuNR@protein dispersions before lyophilization in terms of quality and colloidal stability (Figure 3d). The L-LSPR of the

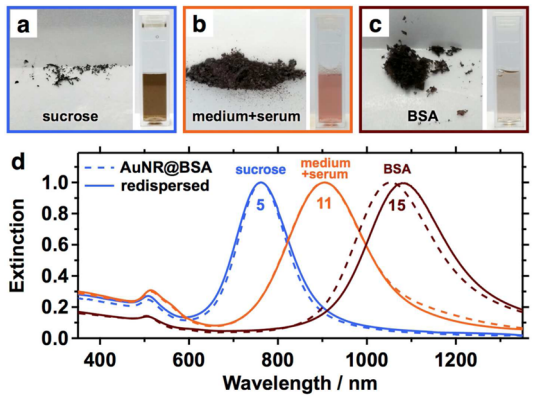

Figure 3. Redispersion behavior of different freeze-dried AuNR@BSA powders: (a) No. 5 with 1 mg/mL sucrose (c_{Au} = 0.34 mM); (b) No. 11 from DMEM+10% NCS (c_{Au} = 0.12 mM); and (c) No. 15 with 1 mg/mL BSA (c_{Au} = 0.16 mM). All powders spontaneously redispersed in water at pH 12 (cuvettes). (d) UV−vis−NIR spectra of AuNR@BSA samples before (dashed line) and after freeze-drying (full line).

sucrose-lyoprotected sample matches perfectly before and after lyophilization. In the case of the BSA-lyoprotected sample, there is a slight red shift after redispersion, which is presumably due to the incomplete redispersion of the dry AuNRs or changes in the local refractive index (changes in coating thickness or density). Furthermore, we lyophilized stable dispersions of AuNR@protein in pure DMEM and in DMEM containing 10% NCS. The powders were light brown in color, due to the high salt and high protein content. Both DMEM-based AuNR@BSA powders redispersed spontaneously upon addition of water (see Video V3 for redispersion behavior of DMEM+10% NCS). Although the pure DMEM dispersions of AuNR@protein were highly stable before lyophilization, the redispersed systems exhibited slight aggregation of the AuNRs. However, the DMEM formulation containing 10% NCS redispersed perfectly, and the AuNR@BSA samples showed the same quality and colloidal stability as before the lyophilization (see Figure 3). It is worth noting that such cell culture media-based dry formulations could directly be used in bioapplications simply by adding water to the ready-made formulation.

Considering the growing interest in AuNRs for biomedical applications, it is highly important to remove CTAB (or CTAC) completely from the particle surface. By coating negatively charged proteins on surfactant-coated positively charged NPs, three possible scenarios can occur: (1) the proteins adsorb on top of the positively charged CTAB bilayer via electrostatic interactions and wrap the AuNR completely; (2) the protein replaces partially the CTAB molecules; and (3) the protein replaces all CTAB molecules completely from the AuNR surface. Hence, to answer the question whether CTAB is still present underneath or within the protein layer after functionalization we performed SERS. Analytical SERS allows for ultrasensitive detection of organic molecules in the vicinity of plasmonic nanostructures.[48−52] In analytical SERS the general notion dictates to aim for maximum enhancement factors by using excitation wavelengths matching the localized surface plasmon resonance of the applied NPs. Since the LSPR depends on particle size, shape, orientation, and aggregation, a broad assortment of excitation sources (lasers) would be required to flexibly adopt for the respective samples of interest.

Figure 4 shows the SERS spectra of AuNR and AuNS with CTAB and BSA coating dispersed in water and compared with conventional Raman spectra of crystalline CTAB and dry solid BSA. In contrast to the reports in literature, where only selected signals (1070 and 1445 cm^{-1}) were used,[53] we evaluated an extended frequency regime to assert the complete replacement of CTAB by BSA. Furthermore, we decided to include spherical NPs[31] in this SERS study providing further validation of the complete exchange of CTAB by BSA at the nanoparticle surface and answering the open question of the previous report.[29] Moreover, we show that also off-resonance measurements, using a standard HeNe laser at 633 nm, allow for the SERS characterization of the ligand shell of NPs. Off-resonance excitation inherently limits the local electromagnetic enhancement to surface-near distances. However, the loss in electromagnetic enhancement can be balanced by measuring at high NP concentrations (up to 20 mg/mL), which can be achieved with protein-coated NPs. At higher concentrations, the total number of scattering events is greatly increased. Additionally, measurements of dispersions take advantage of the continuous flow of NPs through the confocal excitation volume and therewith allow for efficient probing of the NP coating.

The low-frequency domain (Figure 4a) is dominated by the halide counterion signal of surface-bound bromide ($AuBr^-$) at 176 cm^{-1},[53] indicating a surface-bound interlayer of halides between the cetylammonium cation (CTA^+) molecules and the NP gold surface. After BSA coating this signal completely vanished, as expected.

Figure 4b shows the frequency domain attributed to the CN^+ stretching of the trimethylammonium (TMA) headgroup. While crystalline CTAB features three distinct signals at 754, 763, and 774 cm^{-1},[53] the CTAB coatings only show the symmetric stretch at 763 cm^{-1}.[53,54] For BSA-coated NPs this signal is lost, whereas another signal at 750 cm^{-1} arises for the AuNS sample and solid BSA. This signal can be assigned to the

DOI: 10.1021/acsami.5b00335
ACS Appl. Mater. Interfaces 2015, 7, 5984−5991

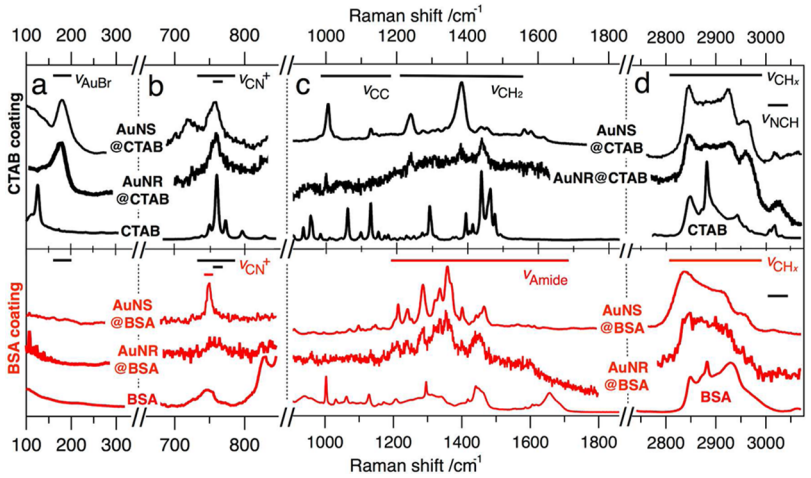

Figure 4. SERS of AuNPs (AuNS: spheres; AuNR: rods) with CTAB (black, upper) and BSA (red, lower) coating dispersed in water and compared with conventional Raman spectra of crystalline CTAB and dry BSA: (a) Counterion signals; (b) ammonium signals; (c) skeletal chain vibrations (upper) and amide bands (lower); (d) methyl/methylene "fingerprint". The spectra are offset, scaled for clarity, and show raw data without background correction.

Table 1. Overview of Characteristic Vibrational Modes of CTAB and BSA Used for Analysis of the Nanoparticle Coatings

	$\nu AuBr^-$ (counterion)	νCN^+	νCC νCH_2 skeletal (chain)	amide bands (protein)	νCH_x	νNCH (headgroup)
Raman shift, cm^{-1}	180	760	1000−1600	1200−1700	2800−3000	3040
CTAB[a]	−	+	+	−	+	+
AuNS@CTAB[b]	+	+	+	−	+	+
AuNR@CTAB[b]	+	+	+	−	+	+
BSA[a]	−	−	−	+	+	−
AuNS@BSA[b]	−	−	−	+	+	−
AuNR@BSA[b]	−	−	−	+	+	−

[a]Conventional Raman measurements of crystalline solids in dry state. [b]SERS measurements of nanoparticles dispersed in water at high concentrations. AuNS: nanospheres; AuNR: nanorods.

aromatic amino acid tryptophan.[55,56] Even though this signal is not well-resolved for AuNR, it can be expected to differ from the distinct CN^+ vibration (TMA, 763 cm^{-1}).

The mid-frequency domain (Figure 4c) of CTAB exhibits a couple of signals characteristic for molecules with long alkyl chains.[53,57,58] These so-called skeletal vibrations are mainly CC (e.g., 1070 and 1144 cm^{-1}) and CH_2 modes (e.g., 1295, 1393, 1447, 1464, and 1481 cm^{-1}). In wet state, as for the CTAB-coated NPs, a reduced amount of signals can be resolved. Besides strong CC stretching vibrations at 1000 and 1144 cm^{-1}, the CH_2 wagging motions at 1232 and 1374 cm^{-1} are most pronounced. The latter signal is expected to partly overlap with strong CH_3 deformations of the headgroup, which would explain the broad peak appearance. The other motions like twisting (~1300 cm^{-1}), scissoring (~1450 cm^{-1}), and symmetric stretching (~1580 cm^{-1}) are of much reduced intensity.[58]

At first glance, the BSA-coated NPs show more condensed midfrequency spectra with strong signals in the 1200 to 1500 cm^{-1} range. Characteristic for proteins are the three amide bands, which reflect combinations of C═O, CN, and NH modes.[55,59] The BSA coating only exhibits the Amide III (CN, NH) at 1295 cm^{-1}. The Amide I (mainly C═O, 1650 cm^{-1}) cannot be resolved, and the Amide II (1550 cm^{-1}) is not present for BSA.[55] Further signals are the CH_2 stretching (near 1450 cm^{-1})[55] and various functional groups of the protein. Though a complete deconvolution is beyond the scope of this analysis, the absence of the distinct skeletal vibrations clearly indicates the successful removal of CTAB from the NP surface.

The high-frequency multiplet of methyl/methylene CH_x vibrations at 2800 to 3000 cm^{-1} may serve as a fingerprint pattern (see Figure 4d). In contrast to earlier studies where these fingerprint modes could not be well-resolved,[53,55,60] we were able to well-resolve distinct patterns for both coatings. The fingerprint pattern consists of four CH stretching vibrations:[54] sym CH_2 at 2850 cm^{-1}, antisym CH_2 at 2880 cm^{-1}, sym CH_3 at 2930 cm^{-1}, and antisym CH_3 at 2960 cm^{-1}. Da Costa and co-workers showed that these modes are almost temperature-insensitive but are very sensitive to environmental and conformational changes.[54] The fingerprint shape reflects the general order/disorder of alkyl chains (intensity ratio of 2880/2850 signals) as well as the polarity of the chain environment (2930/2850 ratio). A high chain order can be found for both crystalline CTAB and solid BSA based on the sharp antisym methylene stretch (2880 cm^{-1}) owing to close packing of planar zigzag chains.[58] The order at the NP surface is reduced owing to the higher mobility of the methylene groups. Furthermore, the sym methyl stretch (2930 cm^{-1}) is a sensor for the polarity at the particle/coating interface. Here, the $AuBr^-$ interlayer of the CTAB-coated NPs exhibits higher polarity than the more hydrophobic gold surface, as seen for BSA-coated NPs. In addition, the absence of the NCH antisym stretching mode at 3040 cm^{-1} next to the multiplet, assigned to the CTA^+ headgroup,[58] further suggests the complete removal of CTAB from the surface.

DOI: 10.1021/acsami.5b00335
ACS Appl. Mater. Interfaces 2015, 7, 5984−5991

Consequently, both AuNS and AuNR give strong evidence for the complete exchange of CTAB by BSA throughout the studied frequency spectrum. The characteristic signals of CTAB and BSA are listed in Table 1. The protein coating resulted in a loss of the counterion ($AuBr^-$), headgroup (CN, NCH), and skeletal chain (CC, CH_2) signals characteristic for CTAB. In lieu of these, distinct signals of the amide bands could be found along with significant changes of the high-frequency fingerprint pattern, as expected.

CONCLUSION

In conclusion, we report on highly stable and surfactant-free protein-coated AuNRs. The colloidal stability is evidenced by UV−vis−NIR spectroscopic characterization of the samples, which show no changes in their LSPRs characteristic for aggregation. The high colloidal stability at very high particle concentrations is maintained at physiological salt concentrations and even in biological media such as DMEM. Moreover, owing to the robust protein coating, such NPs can be lyophilized to powder, similar to proteins. Strikingly, the optical and colloidal properties of the AuNRs are completely maintained upon redispersion. By freeze-drying such particles, long-term storage under ambient conditions and stability could be ensured. Furthermore, the protein-coated AuNRs can be directly freeze-dried in cell culture media containing serum, which can be then redispersed on desire. Such cell culture media-based dry formulations could be directly used in bioapplications simply by adding water to the ready-made formulations.

Most importantly, we showed via SERS that the toxic surfactant CTAB is completely removed from the surface of AuNRs and AuNS. The complete removal of CTAB is a key step toward safe bioapplication of protein-coated NPs. In the context of biotoxicity, the cellular uptake of protein-coated AuNPs and the evolution of their protein corona will be the focus of subsequent studies.

EXPERIMENTAL SECTION

Materials. Silver nitrate ($AgNO_3$, 99.9999%), sodium borohydride ($NaBH_4$, 99%), hydroquinone (HQ, >99%), hydrogen tetrachloroaurate ($HAuCl_4$, >99.9%), ascorbic acid (AA, 99.0%), bovine serum albumin (BSA, 98%), Dulbecco's Modified Eagle's Medium (DMEM, sterile-filtered without phenol red, D5921), newborn calf serum (NCS, sterile-filtered), and sucrose (>99.0%) were purchased from Sigma-Aldrich. Citrate (99%) and 1 M HCl and NaOH solutions were supplied by Grüssing. Cetyltrimethylammonium bromide (CTAB, 99%, 364.45 g/mol, 0.359 mg/kg iodine) was received from Merck KGaA. All chemicals were used as received. Pure-grade solvents and Milli-Q-grade water were used in all preparations.

AuNR Seeds. Seeds were prepared following a procedure published elsewhere.[41] Briefly, to 5 mL of an aqueous 0.2 mM CTAB solution, 5 mL of an aqueous 0.5 mM $HAuCl_4$ solution was added. To prevent CTAB from crystallization the solution was kept at 32 °C. Subsequently, Au ions were rapidly reduced by adding 0.6 mL of an aqueous 0.01 mM $NaBH_4$ under vigorous stirring. Seeds were aged for 30 min at 300 rpm stirring speed. For synthesis with volumes of 1 L seed preparations was scaled to 30 mL.

AuNRs of Low Aspect Ratio. For preparing AuNRs of low aspect ratios a method by Nikoobakht and El-Sayed[39,40] was adopted with small variations. Aqueous solutions (30 mL) containing 0.1 M CTAB and 0.25 mM $HAuCl_4$ using an aqueous 0.1 M Au stock solution were prepared and kept at 32 °C. Subsequently, varied amounts of an aqueous 0.5 mM $AgNO_3$ stock solution were added to adjust the final silver ion concentration (AuNRs Nos. 1−4 and Nos. 6 and 7: 24, 25, 30, 35, 40, and 50 μM) followed by the addition of 195 μL of an aqueous 0.1 M HCl solution to adjust the pH. Next, 112.5 μL of a 0.1 M AA solution were added to reduce the Au^{3+} to Au^{1+} ions accompanied by a color change from yellow to colorless. In the last step, the AuNR growth was initiated by the addition of 300 μL of as-prepared seed solution. The color changed within 10 min to a slight purple. After 24 h at 32 °C, growth was accomplished. Up-scaled synthesis was performed in a volume of 1 L with the same concentration of CTAB, $HAuCl_4$, and AA, respectively, using a final Ag concentration of 40 μM (AuNR No. 5). Nanorod growth was induced with 7 mL of seed solution.

AuNRs of High Aspect Ratios. Gold nanorods with larger AR values (>4) were prepared following a procedure developed by Vigderman and Zubarev.[41] Aqueous 0.1 M CTAB solution (10 mL) containing 0.5 mM $HAuCl_4$ was prepared using an aqueous 0.1 M gold stock solution. Desired amounts of an aqueous 0.1 mM $AgNO_3$ were used to adjust the Ag ion concentration (AuNRs Nos. 8−10 and Nos. 12 and 13: 0.3, 0.6, 0.65, 0.5, 0.5, and 0.5 mM) followed by the addition of 150 μL of an aqueous 0.1 M HQ solution. Color change from yellow to colorless indicated successful reduction of gold ions. As-prepared seed solutions (AuNRs Nos. 1−4 and Nos. 6 and 7: 80, 80, 80, 40, 160, and 320 μL) were added under rapid stirring to induce rod growth. Color change to a slight purple could be observed after 5 h. The solutions were stored at 32 °C for 24 h. Up-scaled syntheses with volumes of 1 L were performed using same concentrations of CTAB, $HAuCl_4$, and HQ, respectively, and a final concentration of Ag of 0.5 mM (AuNRs No. 11) and 0.4 mM (AuNRs No. 15). Synthesis was induced using 24 mL (AuNRs No. 11) and 15 mL (AuNRs No. 15).

AuNS. Spherical gold nanoparticles with a diameter of 80 nm were synthesized as a reference system for SERS studies following a procedure published previously.[31]

Functionalization with BSA. Prior to the BSA coating of CTAB-stabilized nanoparticles the CTAB concentration in dispersions must be adjusted to the CMC of CTAB, that is, 1 mM (NP concentrations were kept identical to the original synthesis). Then, the NP dispersions with adjusted CTAB concentrations were added slowly to the BSA solution under ultrasonication (BSA solution/NP dispersions, 1:1 v/v). The BSA solution contains: BSA (10 mg/mL), 0.02% citrate, pH 7. The NPs were sonicated for 30 min and then centrifuged. Centrifugation parameters need to be adjusted, that is, sample No. 5 at 7000−8000 rcf, No. 11 at 1500−3500 rcf, and No. 15 at 5000−6000 rcf. The supernatant is replaced by the 10× diluted BSA solution, that is, 1 mg/mL BSA, 0.02% citrate, pH 12, and stirred for at least 24 h. Then the particles were washed with basic water (pH 11−12, >4×) via centrifugation and concentrated as desired.

Freeze-Drying. AuNR@BSA samples (3.5 mL) were freeze-dried using sucrose, BSA, DEMEM, or DMEM+10%NCS as lyoprotecting agents. The concentrations were 1 mg/mL for sucrose and BSA. DMEM and DMEM+10%NCS were used as obtained. The nanorods were centrifuged, and the precipitate was redispersed in the respective media. The Au contents of the resulting powders were 42 wt % for sucrose, 5.6 wt % for BSA, and 5.6 wt % for DMEM+10%NCS.

Characterization. UV−vis−NIR spectra were measured with an Agilent Cary 5000 spectrophotometer with an attached Cary Universal Measurement Accessory (UMA). TEM measurements were done on a Zeiss 922 OMEGA EFTEM at a voltage of 200 kV. Zero-loss filtered images were recorded using a bottom-mounted Ultrascan 1000 (Gatan) CCD camera system. Gatan Digital Micrograph 3.9 for GMS 1.4 software was used for image acquisition.

SERS. Surface-enhanced Raman scattering was measured with a confocal Raman microscope (LabRAM Division, HORIBA Jobin Yvon) equipped with a high-resolution grating (1800 grooves/mm), a Peltier-cooled CCD camera (−70 °C, Synapse) and a HeNe laser as excitation line at 633 nm. Spectra were collected by focusing the laser spot at the air/liquid interface of a sessile drop of liquid (100 μL of each solution cast on a glass slide) by using a 100× objective (Olympus, NA 0.9), providing a spatial resolution of ~1 μm^2. Each sample was measured at least three times at positions more than 300 μm apart from each other.

DOI: 10.1021/acsami.5b00335
ACS Appl. Mater. Interfaces 2015, 7, 5984−5991

■ ASSOCIATED CONTENT

Supporting Information

Full-width half-maximum of L-LSPRs; redispersion behavior of lyophilized AuNR@BSA powders with and without additional lyoprotecting agents (images and videos); redispersion after long-term storage (extinction spectra). This material is available free of charge via the Internet at http://pubs.acs.org.

■ AUTHOR INFORMATION

Corresponding Author

*E-mail: munish.chanana@uni-bayreuth.de.

Author Contributions

[§]These authors contributed equally. The manuscript was written through contributions of all authors. All authors have given approval to the final version of the manuscript.

Funding

German Research Foundation (DFG), SFB 840; European Research Council (ERC), ERC-2012-StG 306686 METAMECH.

Notes

The authors declare no competing financial interest.

■ ACKNOWLEDGMENTS

This study was funded by the European Research Council under Grant No. ERC-2012-StG 306686 (METAMECH: Template-assisted assembly of METAmaterials using MECHanical instabilities) and by the German Research Foundation (DFG) within the collaborative research center SFB 840. M.T. was supported by the Univ. of Bayreuth graduate school and by the Elite Network Bavaria in the framework of the Elite Study Program "Macromolecular Science" and funded via a grant for Ph.D. candidates according to Bavarian elite promotion law (BayEFG). The authors would like to thank C. Kunert for TEM measurements. C.K. would like to acknowledge fruitful discussions with Dr. W. Häfner.

■ REFERENCES

(1) Vigderman, L.; Khanal, B. P.; Zubarev, E. R. Functional Gold Nanorods: Synthesis, Self-Assembly, and Sensing Applications. *Adv. Mater.* **2012**, *24*, 4811−4841.

(2) Li, P.-C.; Wang, C.-R. C.; Shieh, D.-B.; Wei, C.-W.; Liao, C.-K.; Poe, C.; Jhan, S.; Ding, A.-A.; Wu, Y.-N. In Vivo Photoacoustic Molecular Imaging with Simultaneous Multiple Selective Targeting Using Antibody-Conjugated Gold Nanorods. *Opt. Express* **2008**, *16*, 18605.

(3) Kah, J. C. Y.; Olivo, M.; Chow, T. H.; Song, K. S.; Koh, K. Z. Y.; Mhaisalkar, S.; Sheppard, C. J. R. Control of Optical Contrast Using Gold Nanoshells for Optical Coherence Tomography Imaging of Mouse Xenograft Tumor Model in Vivo. *J. Biomed. Opt.* **2009**, *14*, 054015−054015−13.

(4) Park, H.; Lee, S.; Chen, L.; Lee, E. K.; Shin, S. Y.; Lee, Y. H.; Son, S. W.; Oh, C. H.; Song, J. M.; Kang, S. H.; Choo, J. SERS Imaging of HER2-Overexpressed MCF7 Cells Using Antibody-Conjugated Gold Nanorods. *Phys. Chem. Chem. Phys.* **2009**, *11*, 7444.

(5) Huang, X.; El-Sayed, I. H.; Qian, W.; El-Sayed, M. A. Cancer Cell Imaging and Photothermal Therapy in the Near-Infrared Region by Using Gold Nanorods. *J. Am. Chem. Soc.* **2006**, *128*, 2115−2120.

(6) Ray, P. C.; Yu, H.; Fu, P. P. Toxicity and Environmental Risks of Nanomaterials: Challenges and Future Needs. *J. Environ. Sci. Health, Part C: Environ. Carcinog. Ecotoxicol. Rev.* **2009**, *27*, 1−35.

(7) Iqbal, M.; Tae, G. Unstable Reshaping of Gold Nanorods Prepared by a Wet Chemical Method in the Presence of Silver Nitrate. *J. Nanosci. Nanotechnol.* **2006**, *6*, 3355−3359.

(8) Basiruddin, S. K.; Saha, A.; Pradhan, N.; Jana, N. R. Functionalized Gold Nanorod Solution via Reverse Micelle Based Polyacrylate Coating. *Langmuir* **2010**, *26*, 7475−7481.

(9) Gole, A.; Murphy, C. J. Polyelectrolyte-Coated Gold Nanorods: Synthesis, Characterization and Immobilization. *Chem. Mater.* **2005**, *17*, 1325−1330.

(10) Liao, H.; Hafner, J. H. Gold Nanorod Bioconjugates. *Chem. Mater.* **2005**, *17*, 4636−4641.

(11) Sendroiu, I. E.; Warner, M. E.; Corn, R. M. Fabrication of Silica-Coated Gold Nanorods Functionalized with DNA for Enhanced Surface Plasmon Resonance Imaging Biosensing Applications. *Langmuir* **2009**, *25*, 11282−11284.

(12) Wijaya, A.; Hamad-Schifferli, K. Ligand Customization and DNA Functionalization of Gold Nanorods via Round-Trip Phase Transfer Ligand Exchange. *Langmuir* **2008**, *24*, 9966−9969.

(13) Orendorff, C. J.; Alam, T. M.; Sasaki, D. Y.; Bunker, B. C.; Voigt, J. A. Phospholipid-Gold Nanorod Composites. *ACS Nano* **2009**, *3*, 971−983.

(14) Vigderman, L.; Manna, P.; Zubarev, E. R. Quantitative Replacement of Cetyl Trimethylammonium Bromide by Cationic Thiol Ligands on the Surface of Gold Nanorods and Their Extremely Large Uptake by Cancer Cells. *Angew. Chem., Int. Ed.* **2011**, *51*, 636−641.

(15) Leonov, A. P.; Zheng, J.; Clogston, J. D.; Stern, S. T.; Patri, A. K.; Wei, A. Detoxification of Gold Nanorods by Treatment with Polystyrenesulfonate. *ACS Nano* **2008**, *2*, 2481−2488.

(16) Huang, H.-C.; Barua, S.; Kay, D. B.; Rege, K. Simultaneous Enhancement of Photothermal Stability and Gene Delivery Efficacy of Gold Nanorods Using Polyelectrolytes. *ACS Nano* **2009**, *3*, 2941−2952.

(17) Prencipe, G.; Tabakman, S. M.; Welsher, K.; Liu, Z.; Goodwin, A. P.; Zhang, L.; Henry, J.; Dai, H. PEG Branched Polymer for Functionalization of Nanomaterials with Ultralong Blood Circulation. *J. Am. Chem. Soc.* **2009**, *131*, 4783−4787.

(18) Chanda, N.; Shukla, R.; Katti, K. V.; Kannan, R. Gastrin Releasing Protein Receptor Specific Gold Nanorods: Breast and Prostate Tumor Avid Nanovectors for Molecular Imaging. *Nano Lett.* **2009**, *9*, 1798−1805.

(19) Alkilany, A. M.; Nagaria, P. K.; Wyatt, M. D.; Murphy, C. J. Cation Exchange on the Surface of Gold Nanorods with a Polymerizable Surfactant: Polymerization, Stability, and Toxicity Evaluation. *Langmuir* **2010**, *26*, 9328−9333.

(20) Lee, S. W.; Kim, B.-S.; Chen, S.; Shao-Horn, Y.; Hammond, P. T. Layer-by-Layer Assembly of All Carbon Nanotube Ultrathin Films for Electrochemical Applications. *J. Am. Chem. Soc.* **2009**, *131*, 671−679.

(21) Takahashi, H.; Niidome, Y.; Niidome, T.; Kaneko, K.; Kawasaki, H.; Yamada, S. Modification of Gold Nanorods Using Phosphatidylcholine to Reduce Cytotoxicity. *Langmuir* **2006**, *22*, 2−5.

(22) Fernández-López, C.; Mateo-Mateo, C.; Alvarez-Puebla, R. A.; Pérez-Juste, J.; Pastoriza-Santos, I.; Liz-Marzan, L. M. Highly Controlled Silica Coating of PEG-Capped Metal Nanoparticles and Preparation of SERS-Encoded Particles. *Langmuir* **2009**, *25*, 13894−13899.

(23) Kim, D. H.; Wei, A.; Won, Y.-Y. Preparation of Super-Stable Gold Nanorods via Encapsulation Into Block Copolymer Micelles. *ACS Appl. Mater. Interfaces* **2012**, *4*, 1872−1877.

(24) Xia, X.; Yang, M.; Wang, Y.; Zheng, Y.; Li, Q.; Chen, J.; Xia, Y. Quantifying the Coverage Density of Poly(Ethylene Glycol) Chains on the Surface of Gold Nanostructures. *ACS Nano* **2012**, *6*, 512−522.

(25) Kinnear, C.; Dietsch, H.; Clift, M. J. D.; Endes, C.; Rothen-Rutishauser, B.; Petri-Fink, A. Gold Nanorods: Controlling Their Surface Chemistry and Complete Detoxification by a Two-Step Place Exchange. *Angew. Chem., Int. Ed.* **2013**, *52*, 1934−1938.

(26) Gu, P.; Birch, D. J. S.; Chen, Y. Dye-Doped Polystyrene-Coated Gold Nanorods: Towards Wavelength Tuneable SPASER. *Methods Appl. Fluoresc.* **2014**, *2*, 024004.

DOI: 10.1021/acsami.5b00335
ACS Appl. Mater. Interfaces 2015, 7, 5984−5991

(27) Chen, Y.-S.; Frey, W.; Kim, S.; Kruizinga, P.; Homan, K.; Emelianov, S. Silica-Coated Gold Nanorods as Photoacoustic Signal Nanoamplifiers. *Nano Lett.* **2011**, *11*, 348−354.
(28) Chanana, M.; Correa-Duarte, M. A.; Liz-Marzan, L. M. Insulin-Coated Gold Nanoparticles: a Plasmonic Device for Studying Metal-Protein Interactions. *Small* **2011**, *7*, 2650−2660.
(29) Strozyk, M. S.; Chanana, M.; Pastoriza-Santos, I.; Pérez-Juste, J.; Liz-Marzan, L. M. Protein/Polymer-Based Dual-Responsive Gold Nanoparticles with pH-Dependent Thermal Sensitivity. *Adv. Funct. Mater.* **2012**, *22*, 1436−1444.
(30) Chanana, M.; Rivera Gil, P.; Correa-Duarte, M. A.; Liz-Marzan, L. M.; Parak, W. J. Physicochemical Properties of Protein-Coated Gold Nanoparticles in Biological Fluids and Cells Before and After Proteolytic Digestion. *Angew. Chem., Int. Ed.* **2013**, *52*, 4179−4183.
(31) Hanske, C.; Tebbe, M.; Kuttner, C.; Bieber, V.; Tsukruk, V. V.; Chanana, M.; König, T.; Fery, A. Strongly Coupled Plasmonic Modes on Macroscopic Areas via Template-Assisted Colloidal Self-Assembly. *Nano Lett.* **2014**, *14*, 6863−6871.
(32) Daniel, M.-C.; Astruc, D. Gold Nanoparticles: Assembly, Supramolecular Chemistry, Quantum-Size-Related Properties, and Applications Toward Biology, Catalysis, and Nanotechnology. *Chem. Rev.* **2004**, *104*, 293−346.
(33) Grzelczak, M.; Pérez-Juste, J.; Mulvaney, P.; Liz-Marzan, L. M. Shape Control in Gold Nanoparticle Synthesis. *Chem. Soc. Rev.* **2008**, *37*, 1783.
(34) Sardar, R.; Funston, A. M.; Mulvaney, P.; Murray, R. W. Gold Nanoparticles: Past, Present, and Future. *Langmuir* **2009**, *25*, 13840−13851.
(35) Klinkova, A.; Choueiri, R. M.; Kumacheva, E. Self-Assembled Plasmonic Nanostructures. *Chem. Soc. Rev.* **2014**, *43*, 3976−3991.
(36) Nie, Z.; Fava, D.; Kumacheva, E.; Zou, S.; Walker, G. C.; Rubinstein, M. Self-Assembly of Metal-Polymer Analogues of Amphiphilic Triblock Copolymers. *Nat. Mater.* **2007**, *6*, 609−614.
(37) Caswell, K. K.; Wilson, J. N.; Bunz, U. H. F.; Murphy, C. J. Preferential End-to-End Assembly of Gold Nanorods by Biotin−Streptavidin Connectors. *J. Am. Chem. Soc.* **2003**, *125*, 13914−13915.
(38) Sethi, M.; Joung, G.; Knecht, M. R. Linear Assembly of Au Nanorods Using Biomimetic Ligands. *Langmuir* **2009**, *25*, 1572−1581.
(39) Nikoobakht, B.; El-Sayed, M. A. Preparation and Growth Mechanism of Gold Nanorods (NRs) Using Seed-Mediated Growth Method. *Chem. Mater.* **2003**, *15*, 1957−1962.
(40) Jana, N. R.; Gearheart, L.; Murphy, C. J. Wet Chemical Synthesis of High Aspect Ratio Cylindrical Gold Nanorods. *J. Phys. Chem. B* **2001**, *105*, 4065−4067.
(41) Vigderman, L.; Zubarev, E. R. High-Yield Synthesis of Gold Nanorods with Longitudinal SPR Peak Greater Than 1200 Nm Using Hydroquinone as a Reducing Agent. *Chem. Mater.* **2013**, *25*, 1450−1457.
(42) Ehlert, S.; Taheri, S. M.; Pirner, D.; Drechsler, M.; Schmidt, H.-W.; Förster, S. Polymer Ligand Exchange to Control Stabilization and Compatibilization of Nanocrystals. *ACS Nano* **2014**, *8*, 6114−6122.
(43) Funston, A. M.; Novo, C.; Davis, T. J.; Mulvaney, P. Plasmon Coupling of Gold Nanorods at Short Distances and in Different Geometries. *Nano Lett.* **2009**, *9*, 1651−1658.
(44) Link, S.; Mohamed, M. B.; El-Sayed, M. A. Simulation of the Optical Absorption Spectra of Gold Nanorods as a Function of Their Aspect Ratio and the Effect of the Medium Dielectric Constant. *J. Phys. Chem. B* **1999**, *103*, 3073−3077.
(45) Link, S.; El-Sayed, M. A. ERRATUM: Simulation of the Optical Absorption Spectra of Gold Nanorods as a Function of Their Aspect Ratio and the Effect of the Medium Dielectric Constant. *J. Phys. Chem. B* **2005**, *109*, 10531−10532.
(46) Pérez-Juste, J.; Pastoriza-Santos, I.; Liz-Marzan, L. M.; Mulvaney, P. Gold Nanorods: Synthesis, Characterization and Applications. *Coord. Chem. Rev.* **2005**, *249*, 1870−1901.
(47) *Cryopreservation and Freeze-Drying Protocols,* 2nd ed.; Day, J. G., Stacey, G. N., Eds.; Springer: New York, 2007; Vol. *368*.
(48) Pazos-Perez, N.; Ni, W.; Schweikart, A.; Alvarez-Puebla, R. A.; Fery, A.; Liz-Marzan, L. M. Highly Uniform SERS Substrates Formed by Wrinkle-Confined Drying of Gold Colloids. *Chem. Sci.* **2010**, *1*, 174−178.
(49) Pazos-Perez, N.; Wagner, C. S.; Romo-Herrera, J. M.; Liz-Marzan, L. M.; Garcia de Abajo, F. J.; Wittemann, A.; Fery, A.; Alvarez-Puebla, R. A. Organized Plasmonic Clusters with High Coordination Number and Extraordinary Enhancement in Surface-Enhanced Raman Scattering (SERS). *Angew. Chem., Int. Ed.* **2012**, *51*, 12688−12693.
(50) Mueller, M.; Tebbe, M.; Andreeva, D. V.; Karg, M.; Alvarez-Puebla, R. A.; Pazos-Perez, N.; Fery, A. Large-Area Organization of pNIPAM-Coated Nanostars as SERS Platforms for Polycyclic Aromatic Hydrocarbons Sensing in Gas Phase. *Langmuir* **2012**, *28*, 9168−9173.
(51) Alvarez-Puebla, R. A.; Liz-Marzan, L. M. SERS Detection of Small Inorganic Molecules and Ions. *Angew. Chem., Int. Ed.* **2012**, *51*, 11214−11223.
(52) Alba, M.; Pazos-Perez, N.; Vaz, B.; Formentin, P.; Tebbe, M.; Correa-Duarte, M. A.; Granero, P.; Ferré-Borrull, J.; Alvarez, R.; Pallares, J.; Fery, A.; de Lera, A. R.; Marsal, L. F.; Alvarez-Puebla, R. A. Macroscale Plasmonic Substrates for Highly Sensitive Surface-Enhanced Raman Scattering. *Angew. Chem., Int. Ed.* **2013**, *52*, 6459−6463.
(53) Lee, S.; Anderson, L. J. E.; Payne, C. M.; Hafner, J. H. Structural Transition in the Surfactant Layer That Surrounds Gold Nanorods as Observed by Analytical Surface-Enhanced Raman Spectroscopy. *Langmuir* **2011**, *27*, 14748−14756.
(54) da Costa, A. M.; Geraldes, C.; Teixeira-Dias, J. Micellar Aggregation of CTAB in Water and Chloroform Solutions—a Study by Laser Raman Spectroscopy. *J. Colloid Interface Sci.* **1982**, *86*, 254−259.
(55) Lin, V. J.; Koenig, J. L. Raman Studies of Bovine Serum Albumin. *Biopolymers* **1976**, *15*, 203−218.
(56) Aliaga, A. E.; Osorio-Román, I.; Leyton, P.; Garrido, C.; Cárcamo, J.; Caniulef, C.; Célis, F.; Díaz F, G.; Clavijo, E.; Gómez-Jeria, J. S.; Campos-Vallette, M. M. Surface-Enhanced Raman Scattering Study of L-Tryptophan. *J. Raman Spectrosc.* **2009**, *40*, 164−169.
(57) Snyder, R. G.; Schachtschneider, J. H. Vibrational Analysis of the N-Paraffins—I. *Spectrochim. Acta* **1963**, *19*, 85−116.
(58) Dendramis, A. L.; Schwinn, E. W.; Sperline, R. P. A Surface-Enhanced Raman Scattering Study of CTAB Adsorption on Copper. *Surf. Sci.* **1983**, *134*, 675−688.
(59) David, C.; Guillot, N.; Shen, H.; Toury, T.; Chapelle, M. L.; de, L. SERS Detection of Biomolecules Using Lithographed Nanoparticles Towards a Reproducible SERS Biosensor. *Nanotechnology* **2010**, *21*, 475501.
(60) Iosin, M.; Toderas, F.; Baldeck, P. L.; Astilean, S. Study of Protein-Gold Nanoparticle Conjugates by Fluorescence and Surface-Enhanced Raman Scattering. *J. Mol. Struct.* **2009**, *924−26*, 196−200.

DOI: 10.1021/acsami.5b00335
ACS Appl. Mater. Interfaces 2015, 7, 5984−5991